Available online at www.sciencedirect.com
SCIENCE DIRECT®
Journal of Nuclear Materials 352 (2006) 233–240
journal of nuclear materials
www.elsevier.com/locate/jnucmat

Plutonium incorporation in phosphate and titanate ceramics for minor actinide containment

X. Deschanels [a,*], V. Picot [a], B. Glorieux [b], F. Jorion [a], S. Peuget [a], D. Roudil [a], C. Jégou [a], V. Broudic [a], J.N. Cachia [a], T. Advocat [a], C. Den Auwer [a], C. Fillet [a], J.P. Coutures [b], C. Hennig [c], A. Scheinost [c]

[a] *DIEC/LMPA, CEA/DEN Valrho Marcoule, BP 17171, 30207 Bagnols-sur-Cèze cedex, France*
[b] *PROMES-CNRS Tecnosud, Rambla de la Thermodynamique, 66100 Perpignan, France*
[c] *ROBL-CRG, ESRF, BP 220, 38043 Grenoble, France*

Abstract

Two ceramics, zirconolite and a monazite–brabantite solid solution (MBss) were studied for the immobilization of minor actinides (Np, Am, Cm) produced by reprocessing spent fuel. Monoclinic zirconolite ($CaZrTi_2O_7$) is a fluorite derivative structure and is the primary actinide host phase in Synroc (a titanate composite). Monazite ($LnPO_4$, where Ln = La, Ce, Nd, Gd, etc.) is a monoclinic orthophosphate containing trivalent cations, and brabantite ($Ca_{0.5}An_{0.5}PO_4$) is an isostructural monazite compound containing tetravalent cations (An = Th and U). The nominal composition of the ceramics studied in this work is $(Ca_{0.87}Pu_{0.13})Zr(Al_{0.26}Ti_{1.74})O_7$ for zirconolite and $(Ca_{0.09}Pu_{0.09}La_{0.73}Th_{0.09})PO_4$ for the monazite–brabantite solid solution. These formulas correspond to 10 wt% PuO_2 loading in each material. XANES spectroscopy showed that the plutonium is tetravalent in zirconolite and trivalent in MBss. Thorium, another tetravalent cation, can be incorporated at 10 wt% ThO_2 in MBss. Aluminum and calcium balance the excess cationic charge resulting from the incorporation of Pu(IV) in zirconolite and Th(IV) in brabantite, respectively. The relative density of the pellets exceeded 90% of theoretical density. The samples exhibited a homogeneous microstructure even if some minor phases, representing less than 2% of the surface area, were detected. The two ceramics are compared in terms of actinide loading, and preliminary results on their long-term behavior are discussed.

PACS: 81.05.Je; 61.82−d

1. Introduction

The minor actinides including neptunium, curium, americium are highly radiotoxic. Two options can be considered following enhanced chemical separation during spent fuel reprocessing. The reference option, transmutation by neutron bombardment in nuclear facilities, would reduce the initial radiotoxic inventory. The second option would be to incorporate the separated actinides into an inorganic matrix ensuring long-term stability [1]. In this context, zirconolite and a monazite–brabantite solid

* Corresponding author. Tel.: +33 4 66 79 60 87; fax: +33 4 66 79 77 08.
E-mail address: xavier.deschanels@cea.fr (X. Deschanels).

0022-3115/$ - see front matter © 2006 Elsevier B.V. All rights reserved.
doi:10.1016/j.jnucmat.2006.02.059

solution (MBss) were selected to quantify their performance under self-irradiation, notably under active conditions. Plutonium was used to simulate the behavior of the minor actinides: its long-lived isotope ^{239}Pu (half-life: 24 000 years) was used to verify the loading capacity of these elements in the proposed structures, and its short-lived isotope ^{238}Pu (87 years) to accumulate irradiation damage in a short time. In addition, plutonium is found at the same oxidation states (III and IV) as the minor actinides Am(III), Cm(III), and Np(III) or Np(IV) in oxide matrices, making it a suitable surrogate for these elements.

Previous work [2–7] has already shown the capacity of the zirconolite and the monazite matrix to accommodate actinide loading. This study compares the performance of the two matrices in terms of minor actinide loading based on the results obtained with plutonium-239. Preliminary results on the irradiation behavior of the materials are also discussed.

2. Plutonium loading schemes in the test matrices

2.1. Zirconolite

The structure of zirconolite-2M is monoclinic (space group C_2/c) with the molecular formula $CaZrTi_2O_7$. Tetravalent elements including the actinides (Np(IV), Pu(IV)) can be incorporated not only at zirconium sites but also calcium sites with charge compensation provided by substituting aluminum for titanium. Trivalent elements including the actinides (Am(III), Cm(III), Pu(III), Np(III)) can also be incorporated at the calcium site with the same type of charge compensation (addition of aluminum at the titanium site) [8]. Depending on the redox conditions and the incorporation scheme, plutonium may be found at trivalent or tetravalent oxidation state in this structure [9–11].

Previous work [1] showed that the crystal structure of zirconolite-2M is conserved between 0.15 and 0.16 unit Pu^{4+} per formula unit at the Zr^{4+} site; the zirconolite-4M superstructure appears at higher values. To prevent this structural change, which could affect the performance of the conditioning matrix, we chose to incorporate Pu at the calcium site. Under these conditions, the limit for the monoclinic structure is about 0.2 unit Pu^{3+} per formula unit for materials produced under reducing conditions [9]. This limit is the same for loading Pu(IV) in this way under oxidizing conditions [9]. In fabricating the ceramics for this study, the quantity of added aluminum was determined by assuming the plutonium was at tetravalent oxidation state, resulting in the nominal composition $(Ca_{0.87}Pu_{0.13})Zr(Al_{0.26}Ti_{1.74})O_7$.

2.2. Monazite–brabantite solid solution

Monazite (MPO_4) has a monoclinic structure (space group $P2_1/n$). It consists of series of alternating tetrahedral PO_4 sites and MO_9 polyhedra that may contain trivalent or tetravalent elements. In this case, loading involves the following substitution: $An^{4+} + Ca^{2+} = 2M^{3+}$ (where An represents an actinide), yielding a brabantite structure. The solid solution between the two isostructural compounds $LaPO_4$ (monazite) and $Ca_{0.5}Th_{0.5}PO_4$ (brabantite) is continuous [12]. Plutonium, americium and curium are incorporated in this structure at trivalent state [13–16]. It should also be possible under certain conditions to reduce Np to trivalent oxidation state [10], but Np(IV) is generally observed [17].

A monazite–brabantite solid solution (MBss) with a nominal composition of $(Ca_{0.09}Pu_{0.09}La_{0.73}Th_{0.09})PO_4$ corresponding to the incorporation of Pu(III) was selected for this study because it is suitable for simultaneously loading trivalent (Pu) and tetravalent (Th) actinides.

3. Experimental

3.1. Fabrication of plutonium-239 doped ceramics

The fabrication process is basically the same for both MBss and zirconolite ceramics doped with plutonium-239 (Table 1). The process was developed in a glove box.

The inactive precursor used to synthesize zirconolite was fabricated by a sol–gel process described in reference [18]. The monazite–brabantite solid solution was fabricated by an oxide process. The precursors were ammonium dihydrogenphosphate ($NH_4H_2PO_4$), calcium carbonate, thorium oxide and lanthanum oxide [19]. The operating conditions for each process step are indicated in Table 1. The precursors and the calcined powder were co-milled in a Retsch MM200 mixer-mill with zirconia grinding jar and balls. For zirconolite the milling operation was carried out in isopropanol, but in view of the difficulties encountered (the grinding jars were not sufficiently leaktight), the MBss was milled dry. The pellets were sintered in air.

Table 1
Fabrication processes for zirconolite and monazite–brabantite pellets doped with ^{239}Pu

Process steps	Zirconolite	Monazite–brabantite
Blending and grinding of precursors with PuO_2	180 min in isopropanol	3 × (15 min at 20 Hz) dry
Calcining	120 min at 1523 K	10 h at 1523 K
Milling of calcined powder	180 min	5 × (20 min at 25 Hz)
Uniaxial press compaction	80 MPa (8 mm dia × 10 mm high, M ≈ 1.5 g)	120 MPa (8 mm dia × 10 mm high, M ≈ 1.5 g)
Sintering	15 h at 1723 K	10 h at 1723 K

3.2. Pellet analysis

Polished cross sections of these samples were examined by scanning electron microscopy (SEM) coupled with X-ray microanalysis (EDX) to ensure their chemical homogeneity. The ceramics were also examined using a Cameca SX50 electron microprobe. The standards used for these analyses were a borosilicate glass specimen containing 2 wt% plutonium for Pu determination (M_α line), $CaSiO_4$ or $CaTiSiO_5$ for Ca and O (K_α line), $ZrSiO_4$, $CaTiSiO_5$ for Ti (K_α line), $KAlSi_3O_8$, GaP (K_α line), LaF_3 (L_α line), Th (M_α line).

X-ray diffraction analysis was also used to determine the presence of any secondary phases. The examination was carried out using a Seifert diffractometer in Bragg–Brentano geometry. A silicon standard was used to adjust the device geometry to ensure an angular position variation of less than 0.02° with respect to the theoretical positions of the main peaks in the compound. The source corresponded to the K_α line of copper; a monochromator was used to eliminate the K_β lines and spurious radiation due to the radioactive environment of the glove box. The spectra were refined by post-processing to determine the angular position of the diffraction peaks before processing using the U-FIT or FullProff program to obtain the structural lattice parameters.

The oxidation state of plutonium was determined in the LURE facility at Orsay University and at the European Synchrotron Radiation Facility (Grenoble, France) by plutonium L_{III}-edge XANES (X-ray Absorption Near-Edge Structure) spectroscopy in fluorescence detection mode.

The sample density was determined from dimensional measurements and weighing.

4. Results

The relative density of the zirconolite and MBss pellets fabricated according to the protocol described above exceeded 92% (Table 2). X-ray diffraction analysis of a sample pellet showed that the desired phase was synthesized in both cases. No secondary phase could be detected using this technique.

A more thorough examination by scanning electron microscopy and X-ray microanalysis (EDX) revealed precipitates of a mixed titanium and zirconium oxide (Fig. 1) containing minimal quantities of plutonium in the zirconolite, and precipitates with a PuO_2 core surrounded by a Pu, P, O phase in the MBss (Fig. 2). This suggests that plutonium oxide

Table 2
Characteristics of ^{239}Pu-doped monazite–brabantite and zirconolite pellets

Characteristics	^{239}Pu zirconolite	^{239}Pu monazite –brabantite
Pellets		
Number	19	19
Density (g cm^{-3})	4.39 ± 0.12	5.12 ± 0.04
Relative density (%)	92 ± 2.7	96 ± 1
Crystal parameters		
a (Å)	12.431 (7)	6.8101 (1)
b (Å)	7.248 (4)	7.0387 (1)
c (Å)	11.33 (3)	6.4915 (1)
β (°)	100.57 (3)	103.390 (1)
V (Å^3)	1003(2)	302.7 (1)
Composition		
Elements (at.%)		
Ca	6.70 ± 0.43	1.75 ± 0.10
Pu	1.13 ± 0.04	1.36 ± 0.16
Zr	8.11 ± 0.12	–
Ti	15.68 ± 0.53	–
Al	2.01 ± 0.04	–
O	66.39 ± 0.21	64.84 ± 0.56
P	–	17.93 ± 0.24
Th	–	1.38 ± 0.09
La	–	12.74 ± 0.30
Secondary phase	Zr, Ti, Pu, O (Pu < 1 at.%)	Pu, P, O (Pu < 10 at.%) and PuO_2
Secondary phase (%)	2	0.5

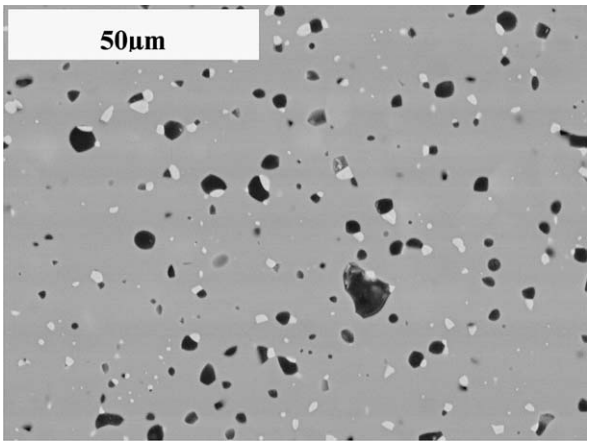

Fig. 1. Microstructure of ^{239}Pu-doped zirconolite. The white secondary phase corresponds to a zone containing Zr, Ti, Pu and O, the dark zone corresponds to porosity, the gray zone corresponds to zirconolite matrix phase.

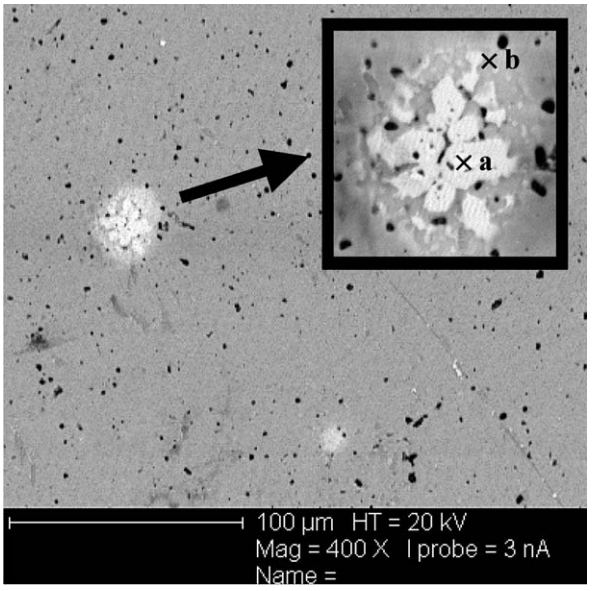

Fig. 2. Microstructure of ^{239}Pu-doped monazite–brabantite ceramic. Inset: enlarged view of a precipitate comprising two phases: one (a) near the composition of PuO_2, the other (b) corresponding to a Pu, P, O phase.

tends to decompose into a Pu–P–O phase before it is fully dissolved in the monazite–brabantite solid solution. In each ceramic the plutonium was uniformly distributed in a major phase as shown by the X-ray distribution map for Pu in a characteristic sample. In the case of zirconolite, the observed secondary phase may be attributable to pollution during powder milling in a planetary zirconia mixer-mill. The presence of a secondary phase in the MBss appears to be the result of insufficient milling of the plutonium oxide during the initial process step.

Plutonium L_{III}-edge XANES spectroscopy analysis was also performed. The resulting spectra were compared with the spectra of reference compounds containing Pu(III) in solution, Pu(IV) in PuO_2 (Fig. 3). Plutonium was found at trivalent oxidation state in MBss, but at tetravalent oxidation state in zirconolite. These findings validate the plutonium loading schemes selected for the two matrices.

The compositions of the zirconolite and MBss ceramics determined by electron microprobe analysis (Table 2) were $(Ca_{0.7}Pu_{0.12})Zr_{0.85}(Al_{0.21}Ti_{1.65})O_7$ and $(Ca_{0.1}Pu_{0.08}La_{0.78}Th_{0.08})P_{1.1}O_4$, respectively, relatively close to the nominal compositions $(Ca_{0.87}Pu_{0.13})Zr(Al_{0.26}Ti_{1.74})O_7$ and $(Ca_{0.09}Pu_{0.09}La_{0.73}Th_{0.09})PO_4$. SEM analysis of the secondary phases confirmed the existence of a mixed zirconium–titanium oxide incorporating a small quantity of plutonium (about 1 at.%) in zirconolite, and of aggregates with a PuO_2 core and a Pu phosphate phase (Pu $<$ 10 at.%) in MBss (Table 2). Image analysis showed that these undesirable phases accounted for only a small fraction of the sample surface area: 2% in zirconolite and 0.5% in MBss (Table 2). Although only a relatively small percentage of secondary phase was observed in the MBss, this proportion must be further diminished when fabricating ^{238}Pu-doped MBss phases, which are rich in plutonium. This should be feasible since, as noted above, the result obtained was most likely due to poor grinding of the precursors with $^{239}PuO_2$. It is unlikely that it corresponds to a Pu loading limit in this structure, as several bibliographical references mention the synthesis of $PuPO_4$ [13,14].

5. Discussion

5.1. ^{239}Pu loading

It is technically feasible to load these ceramics with 10 wt% plutonium oxide. Similar performance can be expected for the minor actinides. It was even possible to incorporate a total of 20 wt% actinide oxides (10 wt% Th oxide and 10 wt% Pu oxide) in MBss. This aspect was not tested for zirconolite.

It is also worth noting that plutonium is incorporated at tetravalent oxidation state in zirconolite. If we consider that a significant fraction of the plutonium is found in the PuO_2 or Pu–P–O secondary phase of the MBss matrix, most likely at tetravalent

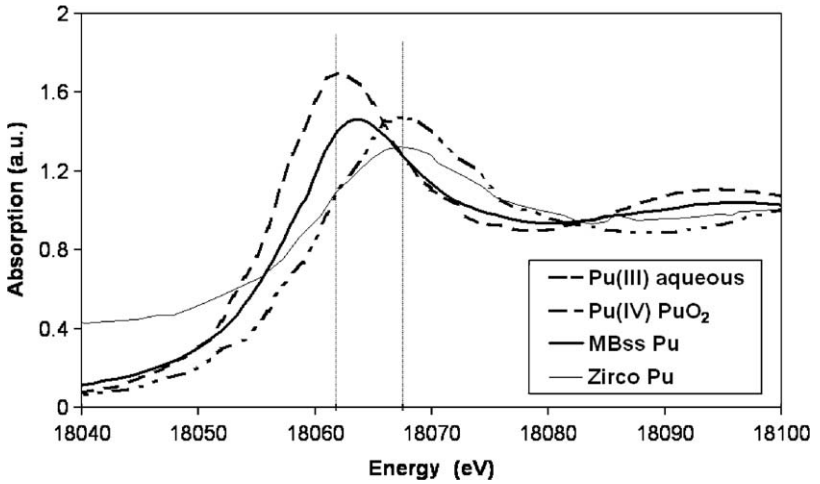

Fig. 3. Comparison of XANES spectra for zirconolite (zirco) and monazite – brabantite (MBss) of references spectra for Pu(IV) and Pu(III) acquired at the Pu L_{III} -edge.

state, it is reasonable to assume that all the plutonium incorporated in the major phase of the MBss is at trivalent state. This is a major difference between the two matrices for plutonium loading. However, for conditioning minor actinides – particularly Np, which is also found at tri or tetravalent oxidation states, reduction to trivalent oxidation state is unlikely since the tetravalent oxidized form is more stable during fabrication in air [17].

5.2. Long-term behavior

Considering the annual amount of radionuclides to be conditioned arising from the reference fuel (UO_2 with a burnup of 45 MW d kg^{-1}) comprises 540 kg of americium, 489 kg of neptunium and 70 kg of curium [20], and given the most likely oxidation states for the minor actinides, i.e., III for Am and Cm, and IV for Np [17], we can determine the nominal composition of the ceramics loaded with 10 oxide wt% minor actinide: i.e., $(Ca_{0.863}Cm_{0.009}Am_{0.067}Np_{0.061})Zr\ (Al_{0.198}Ti_{1.802})O_7$ for zirconolite and $(Ca_{0.04}Cm_{0.006}Am_{0.044}La_{0.87}Np_{0.04})PO_4$ for MBss. Neutron-absorbing elements such as hafnium or gadolinium would also have to be incorporated in the ceramic; although they are not taken into account in the proposed compositions, their feasibility has already been verified [1]. These compositions were used to calculate the integrated doses shown in Fig. 4. Note that there is no significant difference in terms of integrated dose between doped zirconolite and doped MBss containing 10 wt% minor actinide oxides. Moreover,

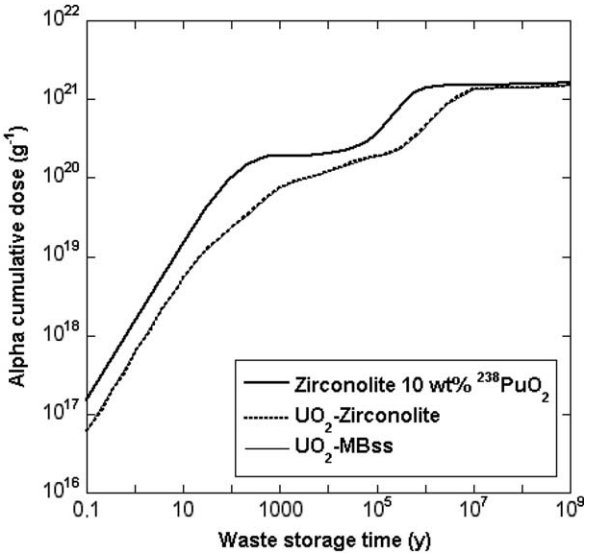

Fig. 4. Comparison of cumulative α-decay dose versus waste storage time for zirconolite pellets doped with 10 wt% of $^{238}PuO_2$ (Pu isotopic composition: 83.6% ^{238}Pu, 14.3% ^{239}Pu, 1.84% ^{240}Pu, 0.11% ^{241}Pu, 0.15% ^{242}Pu) and zirconolite or MBss pellets containing 10 oxide wt% minor actinides in proportions corresponding to the annual radionuclide quantities produced by reprocessing UO_2 spent fuel. Calculations assuming the relative proportions of the relevant isotopes (^{244}Cm, ^{245}Cm, ^{246}Cm, ^{241}Am, ^{243}Am, ^{237}Np) together with their decay products.

the dose integrated by the actual materials (i.e., UO_2–MBss and UO_2–zirconolite) would be only half the dose integrated by pellets doped with plutonium-238. The long-term behavior of these two matrices will be assessed from the results obtained with ^{238}Pu-doped ceramics. Only the zirconolite

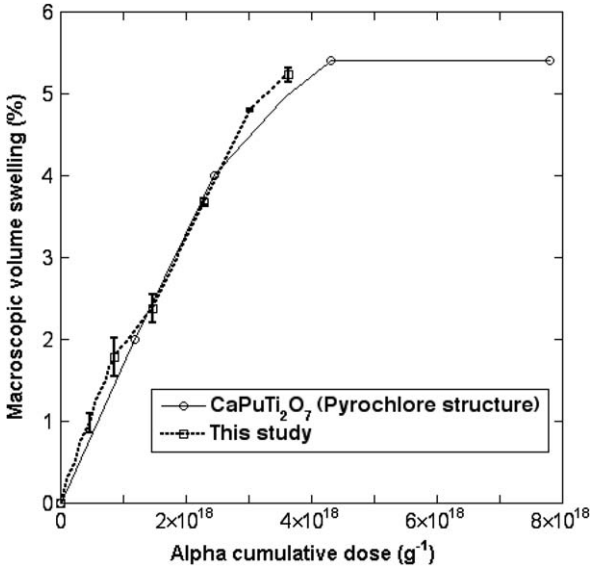

Fig. 5. Macroscopic swelling versus integrated dose for sample stored at room temperature, and comparison with results reported by Clinard [6].

pellets have been fabricated to date, and have now been integrating self-irradiation damage for three years (Fig. 5). The MBss pellets doped with plutonium-238 will be fabricated in the near future. It is therefore impossible at this time to establish direct comparisons between the two materials. Nevertheless, some issues based on data from the literature and on preliminary results are discussed in the following paragraphs.

5.2.1. Behavior under irradiation

Zirconolite is almost completely amorphized after sustaining an integrated alpha dose of about 4×10^{18} g^{-1}; recrystallization of the monoclinic structure occurs above 773 K. The amorphization process has never been observed in natural monazite [21], but has been reported for monazite subjected to external irradiation; recrystallization of these samples occurred at relatively low temperatures (about 573 K) [22]. Burakov [4] reported that the increase of the ^{238}Pu content in monazite structured solid solutions will decrease the resistance of monazite to self-irradiation. $^{238}PuPO_4$ samples became completely amorphous at relatively low dose of about 0.85×10^{18} g^{-1}, whereas (Pu,La)PO_4 remained crystalline up to a cumulative dose of 2.5×10^{18} g^{-1}.

Zirconolite is subject to approximately 5% macroscopic swelling for an integrated alpha dose of about 4×10^{18} g^{-1}; the swelling increases at a lower rate above this value (Fig. 5). The integrated dose corresponding to amorphization is identical with the dose above which macroscopic swelling decelerates; this suggests that both phenomena have the same origin, i.e., the production of point defects in the structure. Clinard [6], working with $CaPuTiO_7$ (pyrochlore structure), obtained swelling comparable to what we have measured, and reached the same conclusions. Swelling resulting from alpha self-irradiation were also observed in ^{238}Pu doped monazite, whereas it was not observed for the (Pu,La)PO_4 solid solutions [4]. Significant swelling occurs in both materials, although the exact figure must still be determined in MBss.

5.2.2. Helium behavior

Helium accumulation in the structures following alpha decay could affect the macroscopic swelling. Above a helium concentration of 0.05–0.1%, major swelling attributed to helium has been observed in various ceramics [23,24]. This phenomenon has not yet been observed in zirconolite doped with plutonium-238 as the amount of helium produced (<200 ppm) is not sufficient. In the case of natural MBss analogs aged 474 ± 1 Ma, one study [21] reported that helium production had a direct effect on swelling and on the occurrence of a subdomain with a monoclinic monazite structure but with different crystal parameters due to preferential incorporation of helium atoms. No precise value was specified for helium-induced swelling, however. Helium behavior can be assessed in plutonium-238 doped ceramics after five to ten years, corresponding to a helium concentration of between about 0.05 and 0.1%.

5.2.3. Chemical durability

In terms of chemical durability, a mean alteration rate of $(1.35 \pm 0.50) \times 10^{-4}$ g m^{-2} d^{-1} was measured in Soxhlet mode at 373 K based on the Pu release from zirconolite specimens doped with plutonium-239 and plutonium-238. The initial leaching data for Pu-doped zirconolite are not significantly different from the data obtained for samples without actinides, and confirm the excellent chemical durability of these ceramics. The leach rate measured on natural MBss analogs aged 500 Ma was also very low: about 10^{-5} g m^{-2} d^{-1} at 343 K for pH values ranging from 2 to 10 [1]. Comparable results were obtained on synthetic monazite $LaPO_4$: about 10^{-3} g m^{-2} d^{-1} at 369 K [25]. Here again, the results must be confirmed with Pu-doped specimens.

Table 3
Number of pellets 8 cm in diameter and 5 cm high produced annually for a minor actinide throughput corresponding to reprocessing of UO_2 fuel

Matrix	Density (g cm^{-3})	Loading (wt%)	Annual matrix mass (kg)	Number of pellets	Total pellets volume (m^3)
Zirconolite	4.5	10	11 000	10 000	2.4
Monazite–brabantite	5	10	11 000	8700	2.2

5.2.4. Conclusion

The overall comparison of the behavior of these ceramics under self-irradiation will be based mainly on the results obtained with ^{238}Pu-doped samples. There is still a lack of data concerning the behavior of Pu-doped MBss samples under self-irradiation, in term of macroscopic swelling, chemical durability and helium release.

5.3. Industrial application

As previously noted, the results obtained with plutonium-doped ceramics suggest that it is reasonable to assume that 10 oxide wt% minor actinides does not represent the limit for these ceramics. Using this value the number of pellets that would have to be fabricated annually to condition the minor actinides produced by reprocessing the reference spent fuel is indicated in Table 3. Ten thousand zirconolite pellets would represent a volume of 2.4 m^3 compared with 2.1 m^3 for 8 700 pellets of monazite–brabantite solid solution. The volume figures are slightly more favorable for MBss, but the difference between the two matrices is not decisive.

6. Conclusions

The results obtained indicate that loading 10 wt% $^{239}PuO_2$ in these ceramics is possible. It was even possible to incorporate 10 oxide wt% ^{239}Pu and 10 wt% thorium oxide in MBss. The density of the resulting materials exceeded 92%. These results confirm previous work [4,6,7]. Neutron-absorbing elements such as Hf or Gd would also be incorporated in the ceramics to prevent the risk of criticality of the waste package.

Plutonium is found mainly at tetravalent oxidation state in zirconolite, and trivalent in MBss. Both ceramics contain a relatively small fraction of precipitated phase (<2% per unit area); this proportion could be further reduced in both cases by optimizing the precursor milling conditions.

Acknowledgment

The authors are grateful to G. Leturcq for synthesizing the inactive precursor used for the fabrication of zirconolite.

References

[1] T. Advocat, C. Guy, CEA technical report DEN/DDIN/DRPG/2001/3 (2002).
[2] L.A. Boatner, G.W. Beall, M.M. Abraham, C.B. Finch, P.G. Huray, M. Rappaz, in: C.J.M. Northrup (Ed.), Scientific Basis for Nuclear Waste Management, 2, Plenum, 1980, p. 289.
[3] N. Dacheux, R. Podor, V. Brandel, M. Genet, J. Nucl. Mater. 252 (1998) 179.
[4] B.E. Burakov, M.A. Yagovkina, V.M. Garbuzov, A.A. Kitsay, V.A. Zirlin, Scientific Basis for Nuclear Waste Management XXVIII, J.M. Hanchar (Ed.), San Franscisco, California, Vol. 824, 219–224, 2004.
[5] Hj. Matzke, W.J. Weber, Radiat. Eff. 98 (1986) 93.
[6] F.W. Clinard, Am. Ceram. Soc. Bull. 65 (1986) 1181.
[7] D.M. Strachan, R.D. Scheele, J.P. Icenhower, E.C. Buck, A.E. Kozelisky, R.L. Sell, R.J. Elovich, W.C. Buckmiller, PNNL Final Report 14588, 2004.
[8] L. Veiller, CEA technical report SRMP-00-04, 2000.
[9] E.R. Vance, C.J. Ball, R.A. Day, K.L. Smith, M.G. Blackford, B.D. Begg, P.J. Angel, J. Alloys Compd. 213/214 (1994) 406.
[10] D.G. Begg, E.R. Vance, S.D. Conradson, J. Alloys Compd. 271–273 (1998) 221.
[11] S.D. Conradson, K.D. Abney, B.D. Begg, E.D. Brady, D.L. Clark, C. Den Auwer, M. Ding, P.K. Dorhout, F.J. Espinosa-Faller, P.L. Gordon, R.G. Haire, N.J. Hess, R.F. Hess, D.W. Keogh, G.H. Lander, A.J. Lupinetti, L.A. Morales, M.P. Neu, P.D. Palmer, P. Paviet-Hartmann, S.D. Reilly, W.H. Runde, C. Drew Tait, D.K. Veirs, F. Wastin, Inorgan. Chem. 43 (2004) 116.
[12] J.-M. Montel, J.-L. Devidal, D. Avignant, Chem. Geol. 191 (2002) 89.
[13] C.E. Bamberger, R.G. Haire, H.E. Hellwege, G.M. Begun, J. Less-Com. Metals 97 (1984) 349.
[14] C.W. Bjorklund, J. Amer. Soc. 79 (1958) 6347.
[15] A.S. Aloy, E.N. Kovarskaya, T.I. Koltsova, S.E. Samoylov, S.I. Rovnyi, G.M. Medvedev, L.J. Jardine, Proceedings of the 8th International Conference on Environmental Management, Bruges, Belgium, 2001, pp. 1833–1836.
[16] K.L. Kelly, G.W. Beall, J.P. Young, L.A. Boatner, in: J.G. Moore (Ed.), Scientific Basis for Nuclear Waste Management Proceedings, 3, Plenum, 1981, p. 189.
[17] A. Tabuteau, M. Pagès, J. Livet, C. Musikas, J. Mat. Sci. Lett. 7 (1998) 1315.

[18] T. Advocat, F. Jorion, T. Marcillat, G. Leturcq, X. Deschanels, J.M. Boubals, L. Bojat, P. Nivet, S. Peuget, Scientific Basis for Nuclear Waste Management XXVII, V.M. Oversby (Ed.), Kalmar, Sweden, vol. 807, 267–272, 2004.
[19] B. Glorieux, F. Jorion, J.M. Montel, X. Deschanels, M. Matecki, J.P. Coutures, Proceedings Atalante 2004 C onference, Nîmes, France, June 21–24, 2004.
[20] X. Deschanels, CEA technical report DEN/DTCD/2004/5, 2004.
[21] A.M. Seydoux-Guillaume, R. Wirth, L. Nasdala, M. Gottschalk, J.M. Montel, W. Heinrich, Phys. Chem. Miner. 29 (2002) 240.
[22] F.G. Karioris, L. Cartz, K.A. Gowda, Radiat. Eff. Lett. 58 (1981) 1.
[23] T. Stoto, Ph.D. thesis, Université d'Orsay, France, 1986.
[24] P. Cheminant, Ph.D. thesis, Université d'Orsay, France, 1997.
[25] L. Bois, M.J. Guittet, F. Carrot, P. Trocellier, M. Gautier-Soyer, J. Nucl. Mater. 297 (2001) 129.